Article

Chemistry & Biology

In-Gel Imaging of RNA Processing Using Broccoli Reveals Optimal Aptamer Expression Strategies

Graphical Abstract

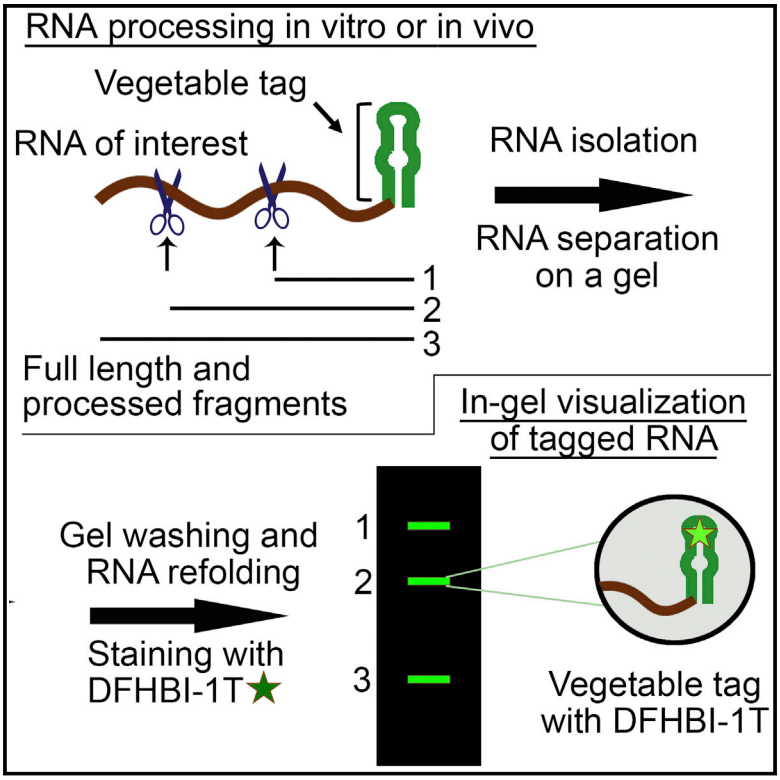

Authors

Grigory S. Filonov, Christina W. Kam, Wenjiao Song, Samie R. Jaffrey

Correspondence

srj2003@med.cornell.edu

In Brief

Filonov et al. describe a technique for simple and sensitive detection of RNA processing by imaging Broccoli-tagged RNAs in gels. Application of this technique enabled the engineering of a three-way junction scaffold (F30) that provides robust expression of RNA aptamers in cells.

Highlights

- F30 is a highly effective RNA scaffold for expressing aptamers in cells
- Commonly used scaffolds for expressing aptamers are prone to intracellular cleavage
- Broccoli and Spinach-tagging enables RNA processing to be easily imaged in gels
- RNAs can be tagged with cassettes containing multiple Broccoli aptamers

Filonov et al., 2015, Chemistry & Biology *22*, 649–660
May 21, 2015 ©2015 Elsevier Ltd All rights reserved
http://dx.doi.org/10.1016/j.chembiol.2015.04.018

CellPress

Chemistry & Biology
Article

CellPress

In-Gel Imaging of RNA Processing Using Broccoli Reveals Optimal Aptamer Expression Strategies

Grigory S. Filonov,[1] Christina W. Kam,[1] Wenjiao Song,[1] and Samie R. Jaffrey[1,*]
[1]Department of Pharmacology, Weill Medical College, Cornell University, New York, NY 10065, USA
*Correspondence: srj2003@med.cornell.edu
http://dx.doi.org/10.1016/j.chembiol.2015.04.018

SUMMARY

RNA aptamers can be expressed in cells to influence and image cellular processes. Aptamer folding is maintained by inserting the aptamers into highly structured RNA scaffolds. Here, we show that commonly used RNA scaffolds exhibit unexpected instability and cleavage in bacterial and mammalian cells. Using an in-gel staining approach for rapid and simple detection of Spinach- or Broccoli-tagged RNAs in cells, we monitored the processing of RNAs tagged with scaffolded aptamers, revealing endonucleolytic cleavage, RNA instability, and poor expression. We reengineered a natural three-way junction structure to generate an alternative scaffold that enables stable aptamer expression in cells. This scaffold was used to create cassettes containing up to four Broccoli units, markedly enhancing the brightness of mammalian cells expressing cassette-tagged RNAs. These experiments describe methods for screening RNA cleavage events in cells and identify cell-compatible scaffolds that enable efficient tagging of RNAs with aptamers for cellular expression.

INTRODUCTION

The SELEX (systematic evolution of ligands by exponential enrichment) technique is a highly effective method for producing RNA aptamers that bind diverse small molecules, proteins, and other biomolecules (Stoltenburg et al., 2007). These aptamers provide the opportunity to manipulate or investigate cellular function. For example, aptamers that bind and inhibit protein function have been developed and have the potential to serve as genetically encoded inhibitors of cellular signaling pathways (Kotula et al., 2014; Seiwert et al., 2000). Other aptamers have been developed that regulate splicing and other processes (Culler et al., 2010; Weigand and Suess, 2007). Aptamers can also be appended to RNAs to enable their purification or imaging. The Spinach, Spinach2, and Broccoli aptamers are RNA mimics of GFP and bind and switch on the fluorescence of a small molecule fluorophore that resembles the GFP fluorophore (Filonov et al., 2014; Paige et al., 2011; Strack et al., 2013). These aptamers have been expressed as fusions with other RNAs, enabling RNA imaging of various RNAs in bacterial and mammalian cells (Filonov et al., 2014; Han et al., 2013; Paige et al., 2011; Pothoulakis et al., 2014; Strack et al., 2013).

A major problem with using RNA aptamers is their poor folding in living cells. Aptamers are highly influenced by flanking sequences, which can interfere with aptamer folding (Martell et al., 2002; Strack et al., 2013). Although screening approaches have been described to improve aptamer folding (Martell et al., 2002), poor aptamer folding is a major roadblock that prevents their widespread use for diverse applications in living cells. Thus, despite their potential utility, aptamers are rarely used to influence or study intracellular processes.

To improve aptamer folding, numerous groups have developed aptamer scaffolds. These are efficiently folding RNAs that contain insertion points for introducing aptamers. The scaffold facilitates folding of the aptamer that is inserted into it. One well-known example is the tRNA scaffold. This scaffold is derived from tRNAs such as the human lysine tRNA ($tRNA^{Lys}_3$) (Ponchon and Dardel, 2007). Aptamers can be inserted into the anticodon stem of the tRNA, which improves their folding. Using this approach, aptamers can be expressed in high quantities for biochemical experiments and crystallization (Muller et al., 2011; Ponchon et al., 2013). This scaffold has also been used for heterologous expression of aptamers in living cells (Paige et al., 2011; Ponchon et al., 2013; Ponchon and Dardel, 2007).

An important feature of the scaffold is that it should be bioorthogonal. This means that the scaffold should not be recognized by intracellular nucleases and targeted for degradation. For example, tRNA precursors are recognized by dedicated RNases, resulting in cleavage near the base of the tRNA (Morl and Marchfelder, 2001). Thus, if the tRNA scaffold is appended to a target RNA, the resulting fusion RNA could be subjected to endonucleolytic cleavage. This could separate the aptamer from the RNA of interest. In addition, since cleaved RNAs are rapidly degraded, scaffold-induced RNA cleavage could reduce the stability of the fusion RNA. Thus, an important criteria when selecting an aptamer scaffold is whether it is a target for undesirable cellular processing.

The compatibility of aptamer scaffolds for eukaryotic expression has not been established. Thus, although RNAs have been expressed as fusions with aptamers scaffolded by $tRNA^{Lys}_3$, the potential cleavage and stability of these RNAs has not been addressed.

The fates of RNAs in cells are usually established by northern blotting to selectively detect specific transcripts in cells. The requirement for optimizing northern blotting conditions, as well as the large number of experiments that may be required for studying RNA cleavage reactions, makes this approach laborious.

Here, we show that RNAs that are tagged with aptamers scaffolded by $tRNA^{Lys}_3$ are targeted for endonucleolytic cleavage in

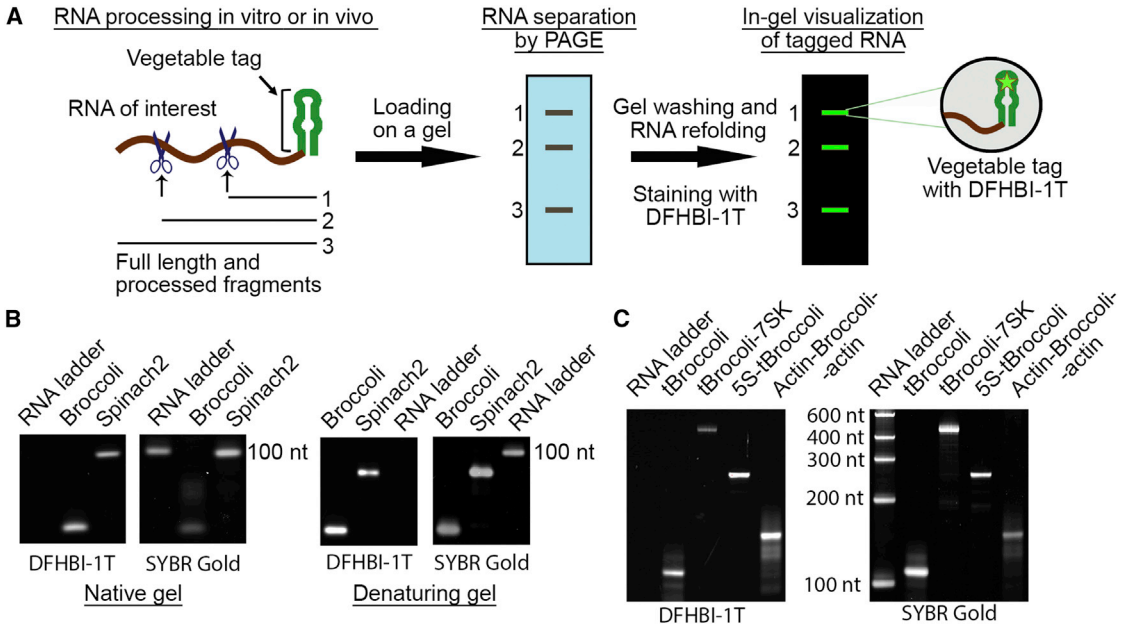

Figure 1. DFHBI-1T-Binding Aptamers Can Be Detected in Gel Alone or in a Context of Other RNAs

(A) Schematic representation of the in-gel detection of vegetable aptamer-tagged RNAs and their cleavage products. In this approach, Spinach, Spinach2, or Broccoli-tagged RNAs and their cleavage products can be simultaneously detected in complex RNA mixtures. For example, a cellular lysate can be queried for different-sized fragments containing a vegetable tag by running the sample on a gel. Use of a denaturing gel can be particularly valuable for accurately determining the size of the RNA fragments. RNAs that contain a vegetable tag can be visualized based on specific binding of DFHBI-1T to the aptamer tag (star and hairpin). Imaging of all the RNA can be subsequently performed by using a nonselective nucleic acid stain.

(B) Broccoli and Spinach2 can be detected using either native or denaturing PAGE. In vitro transcribed Broccoli and Spinach2 were subjected to native or denaturing PAGE. Gels were stained first with DFHBI-1T and subsequently with SYBR Gold.

(C) Flanking sequences do not prevent Broccoli from refolding in the gel after denaturing PAGE (7 M urea). Four RNAs were in vitro transcribed: Broccoli in a context of the aptamer-stabilizing tRNA scaffold (tBroccoli), tBroccoli linked to the 3′ terminus of 5S, tBroccoli linked to the 5′ terminus of 7SK, and Broccoli between fragments of the *β-actin* gene. Each of these RNAs is readily detectable after denaturing PAGE using the protocol described in (B).

bacterial and mammalian cells. To monitor RNA cleavage and to readily compare different scaffolds, we developed an in-gel staining system for rapid and simple detection of RNAs and RNA cleavage products that contain the Spinach or Broccoli aptamer. In this approach, Broccoli-tagged RNAs are selectively detected in total cellular RNA by gel electrophoresis followed by staining of gels with (Z)-4-(3,5-difluoro-4-hydroxybenzylidene)-1,2-dimethyl-1H-imidazol-5(4H)-one (DFHBI), the Broccoli-binding fluorophore. Using this assay, we find that $tRNA^{Lys}_3$-scaffolded aptamers are cleaved from target RNAs, leading to markedly reduced RNA stability. To identify scaffolds that do not impair RNA stability, we tested other scaffolds and identified and reengineered a three-way junction scaffold so that it can be used in bacterial or mammalian cells. RNAs tagged with these scaffolds show substantially increased stability compared with RNAs tagged with the tRNA scaffold. In-gel staining allows simple and rapid characterization of RNA cleavage events and enables the identification of cell-compatible aptamer scaffolds for bacterial and mammalian expression.

RESULTS

Selective In-Gel Imaging of Broccoli and Spinach

Although Spinach and Broccoli can be used to image RNA in living cells (Filonov et al., 2014; Han et al., 2013; Paige et al., 2011), this method does not indicate whether the expressed RNAs are full-length RNAs or have been cleaved. Thus, in order to determine if aptamer scaffolds such as $tRNA^{Lys}_3$ induce RNA cleavage, the RNA cleavage products that are generated in cells need to be detected. Although this is typically done using northern blotting, this technique is time consuming and requires optimization to minimize background labeling.

We wanted to image RNAs and their cleavage products in a rapid and simple manner in order to characterize the stability and cleavage products of diverse aptamer scaffolds. We reasoned that RNAs containing a vegetable aptamer (Broccoli, Spinach, or Spinach2) tag could be imaged using an in-gel staining approach if the aptamer can refold in the gel. In this approach (Figure 1A), an RNA of interest is expressed in cells as a fusion with a vegetable tag. After processing in vitro or in cells, cellular RNA is isolated and resolved by gel electrophoresis. After the vegetable aptamer tag is allowed to refold in the gel, the gel is stained with DFHBI. This allows selective visualization of only the RNAs that contain a vegetable tag. After the tagged RNA is detected, the total cellular RNA can be detected by staining the gel with a nonselective nucleic acid stain.

To test the feasibility of this RNA visualization technique, we first asked if we can detect Spinach2 and Broccoli fluorescence in a gel after electrophoresis. To test this, we in vitro transcribed these RNAs and resolved them by native PAGE. The gel was then

washed with water and stained with DFHBI-1T, which binds to Spinach2 or Broccoli. Fluorescent imaging of this gel revealed bright Spinach2 and Broccoli bands (Figure 1B). Thus, vegetable aptamers can fold and fluoresce in a gel.

To optimize the staining protocol we compared staining with two available fluorophores, DFHBI and DFHBI-1T (Figure S1A). The latter fluorophore is an enhanced version of DFHBI with higher extinction coefficient and that matches filter sets designed for fluorescein isothiocyanate or GFP (Song et al., 2014). Broccoli was resolved by native PAGE and stained with either DFHBI or DFHBI-1T as described above. DFHBI-1T leads to ~100% brighter signal than DFHBI (Figure S1A). Staining was complete after 10–15 min (Figure S1A).

We found that the staining was reversible. After DFHBI-1T staining, the gel was washed with water, which resulted in a complete loss of band fluorescence (Figure S1B). The gel was then stained with SYBR Gold, which nonspecifically stains nucleic acid (Figure S1B). These data show that gels can be rapidly stained with DFHBI-1T and that gels can be subsequently stained with other dyes.

Next, we tested if DFHBI-1T is specific for Broccoli or if it can bind to other G-quadruplex-forming nucleic acids. Broccoli retains most of the residues that form the G-quadruplex that forms the base of the DFHBI-binding pocket in Spinach2 and thus likely has a very similar overall structure (Filonov et al., 2014; Huang et al., 2014; Warner et al., 2014). To test if DFHBI-1T binds other G-quadruplex sequences, we resolved various G-quadruplex-forming RNAs and DNAs by PAGE. DFHBI-1T selectively stains Spinach2 or Broccoli but does not stain any other G-quadruplex or control RNA or DNA (Figures S2A and S2B). The control compound, thioflavin T, which binds to G-quadruplex nucleic acids with high affinity (Renaud de la Faverie et al., 2014), shows relatively nonselective staining of the diverse RNA and DNA G-quadruplexes (Figure S2A). Similarly, DFHBI-1T does not stain cellular RNA, while the G-quadruplex-binders thioflavin T and thiazole orange (Lubitz et al., 2010) both stain numerous endogenous cellular RNAs in bacteria and mammalian cells (Figure S3). These data suggest that DFHBI-1T is highly selective and does not cross-react with structurally similar RNAs.

Next, we asked if the vegetable aptamer tags can be visualized in denaturing gels. Denaturing PAGE allows nucleic acids to be resolved strictly based on their size. Broccoli and Spinach2 were resolved on urea-PAGE gels containing 7 M urea. The gel was then washed with water to remove urea, and RNAs were allowed to refold in presence of DFHBI-1T. Under these conditions, both Broccoli and Spinach2 are readily detectable by fluorescent gel imaging (Figure 1B). The optimal staining/refolding time was again found to be 10–15 min (Figure S4).

We also tested two other DFHBI-binding aptamers, 24-1 and 24-3. These aptamers were discovered in the original SELEX along with Spinach (Paige et al., 2011). Both aptamers are detected in a gel upon DFHBI-1T staining (Figure S5). These data show that various DFHBI-1T-binding aptamers can be refolded in gels for imaging.

In-Gel Imaging of Broccoli-Tagged RNAs

To serve as an in-gel imaging tag, an aptamer should fold well when appended to an RNA of interest. Since Broccoli is the smallest aptamer (~50 nt), we chose it for all subsequent studies. In addition, Broccoli folds efficiently, even without a scaffold (Filonov et al., 2014), which allows comparison with scaffold-free RNAs.

To test if Broccoli can properly fold in a gel when tagged to other RNAs, we generated four constructs with Broccoli and different flanking sequences. First, we inserted Broccoli into the $tRNA^{Lys}_3$ scaffold, which is commonly used to promote RNA aptamers folding in vitro and in cells (Figure S6). The resulting RNA (tBroccoli) was also linked to 3′ terminus of 5S or 5′ terminus of 7SK. Finally, we also generated Broccoli without any scaffold and in the context of ~50-nt *β-actin* transcript sequences linked to both 5′ and 3′ ends. All tested sequences were readily visualized after urea-PAGE (Figure 1C). Thus, Broccoli folds efficiently when placed on either 5′ or 3′ end or inside of a RNA sequence. This suggests that Broccoli can serve as an imaging tag to monitor RNA processing reactions using in-gel RNA imaging.

DFHBI-1T Staining Shows High Sensitivity and Broad Linear Range of Detection

The majority of cellular RNAs are expressed at low levels and their detection requires high imaging probe sensitivity. To test the detection limit of our vegetable tags, we performed a serial dilution of in vitro transcribed 5S-tBroccoli. The detection limit for DFHBI-1T staining is ~1 fmol, which is comparable with the sensitivity of SYBR Gold (Figure 2A) (Tuma et al., 1999). This was unexpected since only one molecule of DFHBI-1T would bind to the aptamer, while many molecules of SYBR Gold would presumably be able to bind along the length of the aptamer. However, the lower autofluorescence of DFHBI-1T allows longer imaging times with nearly undetectable gel background staining.

We next tested signal linearity using a calibration curve (Figure 2B). The calibration curve shows robust linear range down to ~2 fmol, which is again similar to SYBR Gold (Figure 2B). These data strongly suggest that vegetable aptamers, and Broccoli in particular, can be utilized as a sensitive marker for quantification purposes.

tRNA Scaffold Induces 3′ Cleavage in Bacteria

We next sought to use the in-gel imaging system to monitor the effect of different scaffolds on RNA cleavage and stability in cells.

We first tested the $tRNA^{Lys}_3$ scaffold (Ponchon and Dardel, 2007). Although this scaffold is widely used to promote RNA folding, it might be recognized by tRNA processing enzymes, even after an aptamer has been inserted in the anticodon loop.

To test this possibility, $tRNA^{Lys}_3$ containing Broccoli in the anticodon loop (tBroccoli) was expressed in LMG194, Rosetta, and BL21 Star (DE3) *Escherichia coli* strains. In these cases, tBroccoli was transcribed from a plasmid off a T7 or araBAD promoters, and using the T7 transcription terminator. The T7 terminator is transcribed and is a part of all RNAs generated using these promoters. The expected size of the RNA product is 160 nt. DFHBI-1T and then SYBR Gold staining of total bacterial RNA revealed two major bands. The higher molecular weight band had the expected size of ~160 nt. However, a much more prominent lower molecular weight band was detected, which had a size of ~110 nt. This length corresponds to tBroccoli

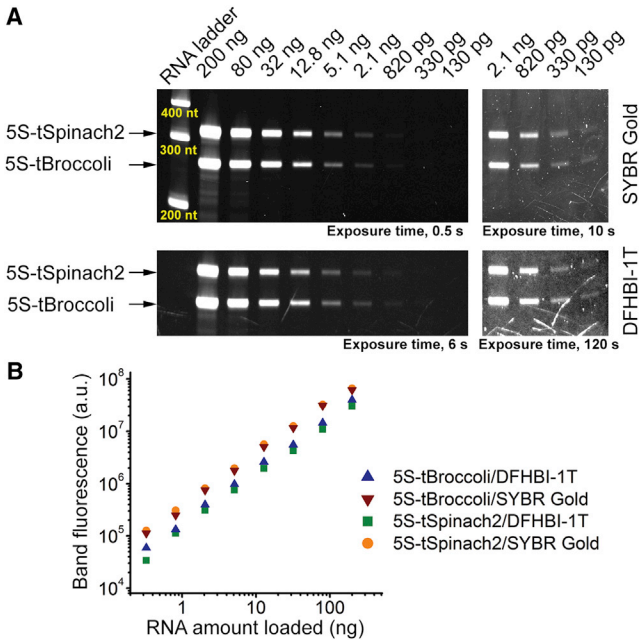

Figure 2. Sensitivity and Linearity of Broccoli-Based In-Gel RNA Detection

(A) To determine DFHBI-1T staining sensitivity, we prepared a serial dilution of in vitro transcribed 5S-tBroccoli or 5S-tSpinach2. The RNA was resolved by urea-PAGE followed by staining with DFHBI-1T and SYBR Gold. Both types of staining showed similar sensitivity with the ability to detect as little as 100–200 pg (~1 fmol) of RNA.

(B) The gel from (A) was used to plot the calibration curve. Both DFHBI-1T and SYBR Gold show excellent linearity down to 300 pg (R^2 for both dyes and both aptamers is ~0.998). The bands from the gel on panel were quantified and the resulting values were plotted on a log scale. a.u., arbitrary units.

alone (114 nt) without the 3′ T7 terminator sequence. This suggests that the RNA is cleaved on the 3′ side of the tRNA.

Interestingly, the ratio of unprocessed/processed tBroccoli appears to depend on the expression time and strength of the promoter/strain. The LMG194 strain has lower expression levels and requires 16 hr for expressing RNA to the level comparable with that of the other strains. However, this longer expression time resulted in all of the transcript being cleaved and no observable full-length transcript. On the other hand, some uncleaved transcript was detected in the other two *E. coli* strains. In both of these strains, a 4-hr induction time was used to detect the transcript. This high-level expression may oversaturate the RNA cleavage pathways needed to generate the truncated transcript.

A possible RNA cleavage pathway is presented in Figure 3B. Based on the known processing pathways for bacterial tRNA (Morl and Marchfelder, 2001), the first step in tBroccoli processing is likely to be endonuclease RNase E cleavage of the downstream sequence followed by trimming at the 3′ terminus by exonucleases RNase T and RNase PH. The minor bands observed above the lower molecular weight tBroccoli band are likely to be intermediate products.

To determine if the major, lower molecular weight band is indeed tBroccoli with the downstream sequences cleaved off, we excised this band from the gel and cloned the eluted RNA. Sequencing of the resulting cDNA showed that this band is tBroccoli with no additional flanking sequences (Figures S7A and S7B).

Next, we tested if the tRNA processing is associated specifically with Broccoli or if it occurs for other aptamers as well. For that, we expressed tSpinach2 and tdBroccoli (dimeric Broccoli in tRNA). Each transcript was expressed in *E. coli* and again analyzed for RNA processing. In-gel staining showed that both tSpinach2 and tdBroccoli underwent RNA cleavage to a similar shortened form, indicating that RNA cleavage is mediated by the tRNA scaffold and not the aptamer fused to it (Figure S8).

Finally, we sought to show that Broccoli itself does not induce RNA cleavage. We expressed Broccoli without the tRNA scaffold and analyzed total RNA. The data show that the expected full-length transcript (98 nt) was the only product observed (Figure 3C). Thus, the tRNA scaffold, and not Broccoli, is the trigger for RNA cleavage by bacterial enzymes. Overall, these data indicate that RNAs tagged with aptamers scaffolded by $tRNA^{Lys}_3$ may be subjected to unanticipated and undesired cleavage reactions in *E. coli*.

The tRNA Scaffold Is Targeted by Endonucleases in Mammalian Cells

We next wanted to determine if tRNA scaffold processing could be monitored in RNA extracts from mammalian cells. We first wanted to determine if Pol II or Pol III promoters express RNA at sufficient levels for detection using the in-gel staining approach. To test this, HEK293T cells were transfected with plasmids expressing Broccoli constructs from either a Pol II or a Pol III promoter. The Pol III promoter was the 5S promoter, which has been frequently used for heterologous RNA expression in mammalian cells (Good et al., 1997). For the Pol II promoter, we used the sno-lnc expression system (Yin et al., 2012), which uses the cytomegalovirus promoter to generate an RNA that is spliced to form a stable intron. The sensitivity of the in-gel staining technique was sufficient to detect RNA produced from either promoter, although the 5S expression was noticeably higher (Figure S9). Since Pol III expression systems are more commonly used, we performed our optimization experiments using these plasmids.

We next asked if the tRNA scaffold is cleaved when expressed in mammalian cells. We assessed the cleavage of Broccoli and tBroccoli transcribed from two different promoters, 5S and U6, in HEK293T cells (Figures 4A–4D). tBroccoli, or Broccoli, expressed from both constructs had a Pol III transcription terminator on the 3′ terminus. The U6 promoter-expressed aptamers have the first 27 nucleotides of the U6 RNA (U6+27) on the 5′ terminus (Good et al., 1997), while aptamers expressed from 5S promoter are linked to the 3′ terminus of 5S rRNA (Paul et al., 2003). Urea-PAGE of total cellular RNA demonstrated that Broccoli without the tRNA scaffold is expressed as a single band of the expected size. However, tBroccoli-containing constructs exhibited other bands in addition to full-length products of the expected size (~260 nt for 5S-tBroccoli and ~170 nt for U6+27 tBroccoli) (Figure 4A). Thus, the tRNA scaffold does not result in a single RNA product in cells.

The shorter RNA fragments could derive from endonucleolytic cleavage of the full-length RNA or could reflect internal

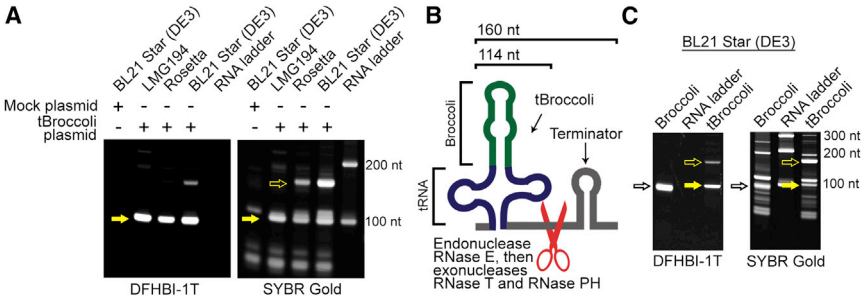

Figure 3. The tRNA Scaffold Triggers RNA Cleavage in *E. coli*

(A) Aptamers with the tRNA scaffold are processed into two forms in *E. coli* and the ratio of these forms depends on the bacterial strain. We induced the expression of tBroccoli from pBAD E tBroccoli or pET28c-tBroccoli in LMG194, Rosetta, and BL21 Star (DE3) strains of *E. coli*. tBroccoli in all strains shows a major fluorescent form of ~110 nt (filled arrow), which is 50 nt shorter than the expected full-length RNA expressed from the plasmid. However, some strains also revealed the presence of a longer RNA (~160 nt, open arrow) that was consistent with the expected size.

(B) tRNA scaffold processing explains presence of two bands in *E. coli*. tBroccoli is recognized as bacterial tRNA, resulting in the 3′ portion of the transcript distal to the tRNA being cleaved off as a part of tRNA maturation process. Thus, the tBroccoli transcript is highly processed, with only levels of the full-length product detectable.

(C) Broccoli without the tRNA scaffold does not get cleaved. In this experiment, we expressed either Broccoli or tBroccoli from the pET28c plasmid in the BL21 Star (DE3) strain. The full-length Broccoli transcript is 98 nt (open arrow). Unlike the tBroccoli transcript, which is highly cleaved (open and filled arrows), the Broccoli transcript is uncleaved, as shown by just one band on the gel. No other smaller products are detected.

transcription initiation from the tRNA itself. Indeed, a tRNA promoter is located within the tRNA scaffold (Chang et al., 2002; Schramm and Hernandez, 2002). To test this, we expressed tBroccoli without using the U6 promoter. This resulted in weak transcription from the tRNA promoter (Figure S10). The full-size product of the expected size was also apparently cleaved to remove the terminator downstream of the tRNA scaffold. However, analysis of the bands suggests that the initial full-length product transcribed from the tRNA promoter is not present in cells expressing U6+27-tBroccoli (Figure S10). Overall, this suggests that the shorter forms of tBroccoli are mostly the result of RNA cleavage, but cryptic initiation from the tRNA can also lead to shorter transcripts as well.

Shorter forms were also observed if dBroccoli or Spinach2 was inserted into the tRNA scaffold, indicating the cleavage is not specific to Broccoli (Figure S11). These data indicate that the tRNA scaffold is recognized and targeted for endonucleolytic cleavage in mammalian cells.

Next, we asked if we can assign each observed band to a specific step in the tRNA processing pathway. The band pattern for both 5S-tBroccoli and U6+27-tBroccoli suggests the following possible order of events (Figures 4A and 4B): RNase P-induced cleavage occurs 5′ to the tRNA, producing a 140-nt product (band 1). Then, another endonuclease, potentially RNase Z, cleaves on the 3′ side of the tRNA, generating tBroccoli (114 nt, band 2) (Phizicky and Hopper, 2010). The faint band observed above band 1 in the case of U6+27-tBroccoli could be explained by an additional intermediate processing event. Alternatively, it can be explained by a reverse order of processing, with RNase Z acting first and generating a U6+27-Broccoli fragment with an expected length of ~155 nt. Finally, there is a faint band (3) running around 70 nt (Figures 4A and 4B). This potentially can be a product of tBroccoli splicing with the tRNA scaffold being recognized as the tRNA exon and Broccoli excised as an intron (Phizicky and Hopper, 2010).

To test the hypothesized order of the cleavage events, we eluted the shorter forms of 5S-tBroccoli RNA from the gel (Figure S7A). Sequencing of the resulting cDNA showed that band 1 results from the cleavage of 5S rRNA, while band 2 results from subsequent cleavage of the sequence downstream of the tRNA (Figure S7C; Figure 4B). Overall, these experiments indicate that the tRNA scaffold induces unexpected cleavage of the RNA into which it is inserted.

tRNA Processing Shows a Precursor-Product Relationship

We next sought to further confirm that the RNA fragments are cleavage products of the initially transcribed RNA. Thus, we sought to determine if RNAs containing the $tRNA^{Lys}_3$ scaffold undergo conversion to shorter products in vitro, thus establishing a precursor-product relationship.

To test this, we examined 5S-tBroccoli RNA cleavage in HEK293 nuclear extracts. In vitro transcribed 5S-tBroccoli was subjected to in vitro processing for up to 3 hr at 37°C. RNAs were isolated and run on urea-PAGE to visualize RNA cleavage products (Figures 5A and 5B). Incubation resulted in discrete cleavage products. At early time points, the major product (1) is ~230 nt, which corresponds to 5S-tBroccoli without the 3′ terminator. The putative tBroccoli band (2) is very faint. At later time points, the major band is ~70 nt and similar to the band 3 seen in Figure 4A, which may reflect the excised Broccoli intron mentioned above. The majority of other bands are more difficult to interpret and could be nonspecific degradation products. Overall, the in vitro result shows several bands that are seen in cells, although the nuclear extract appears to show RNase Z acting first. These data also support that the tBroccoli-containing cleavage products derive from the initial full-length precursor RNA.

To further confirm that tRNA structures are targeted for endonucleolytic cleavage, we used Broccoli-MALAT1. MALAT1 contains a tRNA-like structure called the 3′ mascRNA that is recognized and cleaved off by RNase P in cells and in vitro (Wilusz et al., 2008). We tagged a fragment of human MALAT1 RNA containing its physiological 3′ mascRNA to Broccoli. Indeed, incubation of this RNA with nuclear extract results in a product consistent with cleavage by RNase P at the 5′ side of the mascRNA (Figures S12A and S12B). Thus, tRNA motifs are highly susceptible to cleavage and may be problematic for use as a scaffold due to their efficient targeting by endogenous endonuclease pathways.

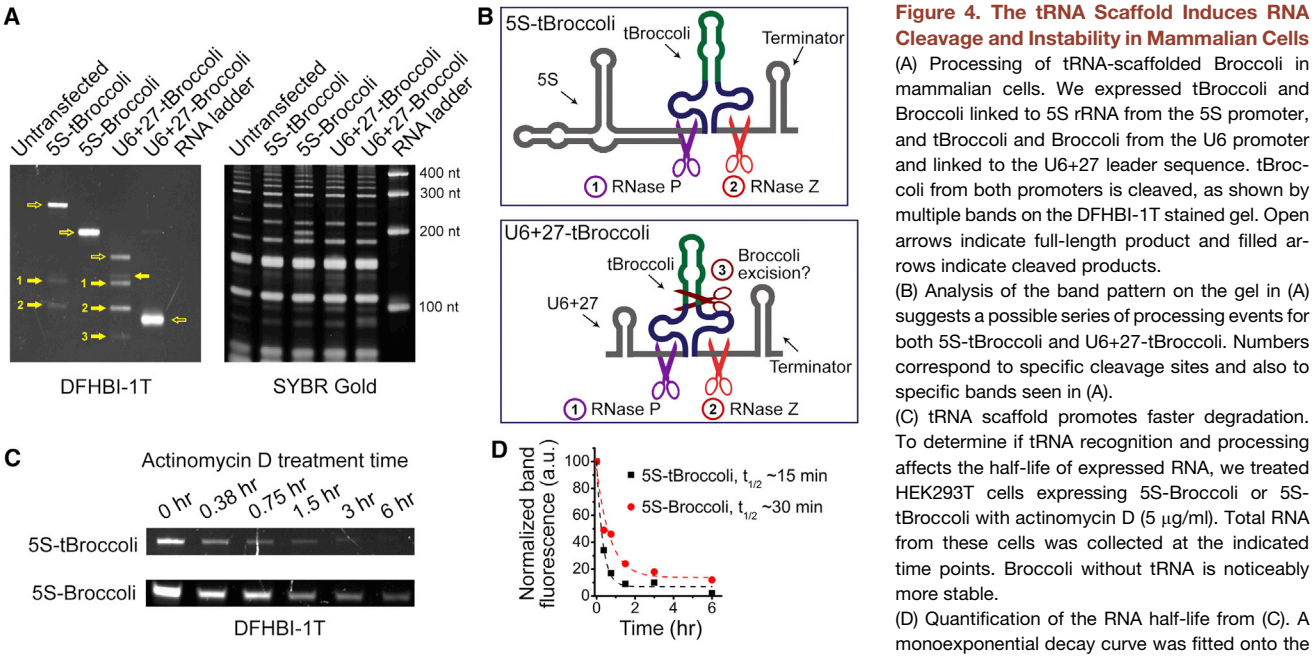

Figure 4. The tRNA Scaffold Induces RNA Cleavage and Instability in Mammalian Cells

(A) Processing of tRNA-scaffolded Broccoli in mammalian cells. We expressed tBroccoli and Broccoli linked to 5S rRNA from the 5S promoter, and tBroccoli and Broccoli from the U6 promoter and linked to the U6+27 leader sequence. tBroccoli from both promoters is cleaved, as shown by multiple bands on the DFHBI-1T stained gel. Open arrows indicate full-length product and filled arrows indicate cleaved products.

(B) Analysis of the band pattern on the gel in (A) suggests a possible series of processing events for both 5S-tBroccoli and U6+27-tBroccoli. Numbers correspond to specific cleavage sites and also to specific bands seen in (A).

(C) tRNA scaffold promotes faster degradation. To determine if tRNA recognition and processing affects the half-life of expressed RNA, we treated HEK293T cells expressing 5S-Broccoli or 5S-tBroccoli with actinomycin D (5 μg/ml). Total RNA from these cells was collected at the indicated time points. Broccoli without tRNA is noticeably more stable.

(D) Quantification of the RNA half-life from (C). A monoexponential decay curve was fitted onto the data points. The SYBR Gold-revealed 5S rRNA band was used for loading normalization. a.u., arbitrary units.

RNAs Tagged with the tRNA Scaffold Are Unstable in Cells

We also considered the possibility that RNA cleavage leads to RNA instability and subsequently reduced expression levels. In many cases, the scaffolded aptamer exhibits a function within the cell, and high concentrations are needed to have a functional effect. However, RNA cleavage is typically associated with rapid RNA degradation due to exonucleases that target RNAs with unprotected 5′ and 3′ ends.

To test this idea, we expressed 5S-tBroccoli and 5S-Broccoli in HEK293T cells and treated the cells with actinomycin D to inhibit nascent transcription. The stability of the tagged RNAs was determined by quantifying the levels of residual tagged RNA at various time points after transcription inhibition (Figure 4C). The 5S RNA containing the tRNA scaffold had a half-life of ~15 min, compared with ~30 min for the 5S RNA that was tagged with Broccoli without tRNA (Figure 4D). Thus, the cleavage induced by tRNA also leads to RNA instability. Thus, the tRNA scaffold, while providing potential benefits for aptamer folding, can also lead to undesirable recognition, cleavage, and, as a result, higher degradation rate and lower expression level.

V5 and F29 as Alternative Scaffolds for RNA Aptamers in Cells

We next asked if scaffold-induced RNA cleavage was also seen with other scaffolds. Two additional scaffolds have recently been described: the *Vibrio proteolyticus* 5S rRNA scaffold (denoted by us as V5) (Zhang et al., 2009) and the Φ29 RNA three-way junction motif (denoted by us as F29) (Shu et al., 2014). V5 is similar to the endogenous bacterial 5S RNA except a specific stem-loop structure was removed to provide an insertion point for aptamers (Zhang et al., 2009). F29 contains a three-way junction, which is an RNA motif seen in naturally occurring riboswitches and viral RNAs (Shu et al., 2014).

We asked if V5 and F29 scaffolded aptamers are recognized and processed in cells. V5- and F29-Broccoli (Figures S13A, S13B, S13D, and S13E) were expressed in *E. coli*, and total RNA was analyzed by urea-PAGE (Figure 6A). RNA was expressed using the T7 promoter as described above. Both V5-Broccoli and F29-Broccoli are highly fluorescent on a DFHBI-1T stained gel, indicating that Broccoli folding is preserved in these scaffolds. V5-Broccoli showed both the full-length product (178 nt) and a shorter fragment consistent with the cleavage downstream of the V5 scaffold. Thus, the V5 scaffold is processed in *E. coli*, although at a much lower level than the tRNA scaffold. The F29-Broccoli was detected primarily as the full-length product with the expected size of 154 nt. A shorter band was observed, but it was present at ~10% of the full-length product. Thus, of the three tested scaffolds, F29 is the most attractive option for the fusion of scaffolded aptamers to RNAs of interest in *E. coli*.

We next expressed V5- and F29-Broccoli in mammalian cells. Both of them were expressed off the U6+27 promoter as described above. Analysis of the total RNA from HEK293T cells expressing V5-Broccoli revealed the expected full-length ~180-nt transcript (Figure 6B). No other bands were observed. HEK293T cells expressing F29-Broccoli showed two bands. One was consistent with the full-length transcript (~160 nt). The other band was ~90 nt (Figure 6B).

We asked if either V5 or F29 impairs RNA stability. To test this, we treated cells with actinomycin D and assessed the amount of Broccoli-tagged RNA at different time points. The half-lives for full-length V5-Broccoli and F29-Broccoli were ~50 min and ~80 min, respectively (Figure 6C; Figure S14).

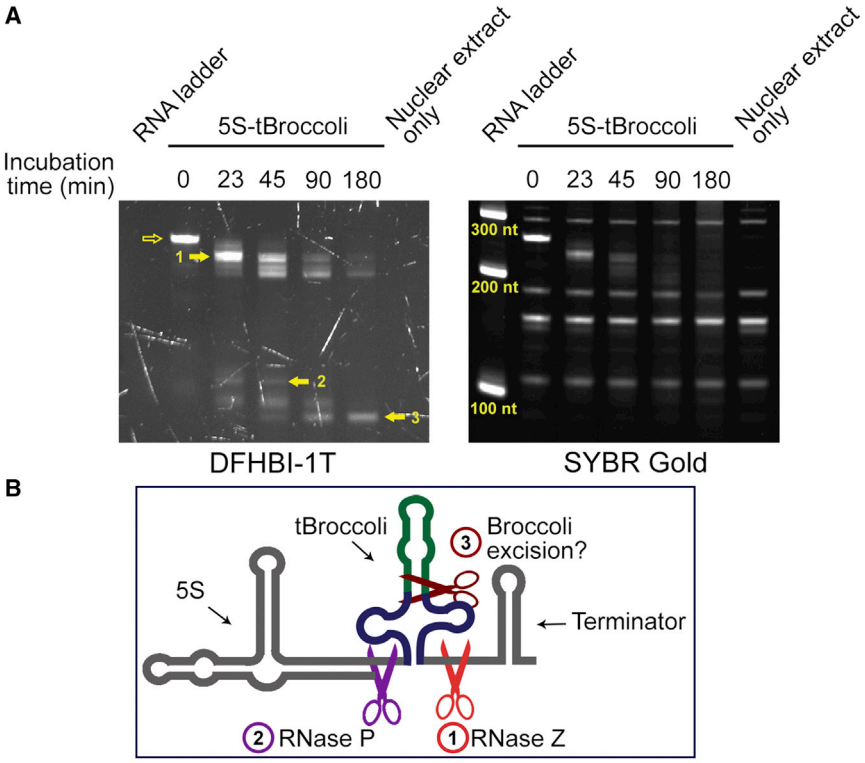

Figure 5. 5S-tBroccoli Processing In Vitro in Mammalian Nuclear Extracts

(A) To further confirm that the processing of tBroccoli is due to cleavage events, we wanted to establish a precursor-product relationship. Thus, we added full-length transcript and observed whether it undergoes cleavage in vitro. In vitro transcribed 5S-tBroccoli was incubated with HEK293 nuclear extracts (Active Motif) for the indicated times. As can be seen, 5S-tBroccoli is cleaved in a time-dependent manner, which can be attributed to both specific processing (bands, labeled with 1, 2, 3) and non-specific degradation. Open arrows indicate full-length product and filled arrows indicate cleaved products.

(B) Schematic representation of the possible order of events in vitro. In vitro processing, unlike in cells, apparently starts with 3′ terminus cleavage with RNase Z, then proceeds via 5′ terminus cleavage with RNase P and finally generates a short fragment, which can be attributed to Broccoli excised as a result of the tRNA splicing process. Steps 1, 2, and 3 correspond to the bands on the gel in (A) labeled with the same numbers. RNase P seems to be less active in vitro compared with in cells as the band 2, presumably generated by the cleavage with this enzyme, is very faint.

Unscaffolded Broccoli exhibited a half-life of ~30 min (Figure 6C), which was similar to that of 5S-Broccoli. Each of these transcripts is substantially more stable than Broccoli transcripts scaffolded by tRNA (see Figure 4D). Overall, these experiments identify V5 and F29 as scaffolds that do not destabilize RNA but instead seem to increase RNA stability and can be used for tagging RNAs in mammalian cells.

Engineering the F30 Scaffold from F29

F29 is an attractive scaffold due to its high structural stability and its ability to accommodate multiple aptamers (Shu et al., 2014). However, as shown above, F29 is not suitable for scaffolding aptamers in mammalian cells since two forms are seen: the full-length aptamer-scaffold fusion and a second lower molecular weight product. Thus, we sought to identify the reason of the formation of the second band and to reengineer F29 so that a single RNA band is seen in mammalian cells.

We noticed that the nucleotide sequence of F29 contains a UUUGUU sequence, which is similar to the Pol III transcription terminator (Figure 7A; Figure S13B; Figure S15). The predicted size of an RNA that terminates at this sequence (~110 nt) matches the length of the second band on the gel (Figure 6B). We therefore sought to mutate this sequence while preserving the structure of the F29 aptamer.

To mutate the putative terminator sequence, we examined the crystal structure of F29 (Zhang et al., 2013). The structure suggested two options for mutagenizing the UUUGUU sequence (Figure S15). First, we mutated the central U (U76) in the three-U stretch to C generating F29mut1. The crystal structure shows that this base is flipped out and does not participate in interactions within the three-way junction core. Second, we changed the first U (U79) in the two-U stretch. Since this nucleotide participates in a base pair, we mutated it to A and also changed the complementary nucleotide to U to maintain the stem. This generated F29mut2.

To test if these mutations blocked the formation of the second band, F29mut1-Broccoli and F29mut2-Broccoli were expressed in HEK293T. To better resolve all the bands, we ran the samples on 10% urea-PAGE (Figure 7B). Under these conditions, we noticed that the second, lower molecular weight band of F29-Broccoli actually consists of two closely running bands. This could be explained by transcription termination on either the three-U stretch or the two-U stretch. In agreement with our hypothesis, F29mut1-Broccoli and F29mut2-Broccoli prevented either one or the other of these closely running bands (Figure 7B). Thus, our data suggest that the formation of the lower molecular weight species of F29 is indeed caused by premature transcription termination.

To prevent transcription termination, we decided to combine both of these successful mutations to generate a scaffold devoid of any unwanted termination products. Combining the mutations in F29mut1 and F29mut2 resulted in a scaffold denoted F30 (Figure S13C and S13F). Analysis of F30-Broccoli expression in mammalian cells and in bacteria shows no or little sign of the lower molecular weight band (Figure 7B; Figure S16A). Thus, F30 is a bioorthogonal scaffold with potentially beneficial properties for aptamer expression in both bacterial and mammalian cells.

Testing the Function of Aptamers Scaffolded by F30 in Mammalian Cells

We first wanted to know if the mutations introduced into F29 to generate F30 impaired its ability to scaffold the folding of

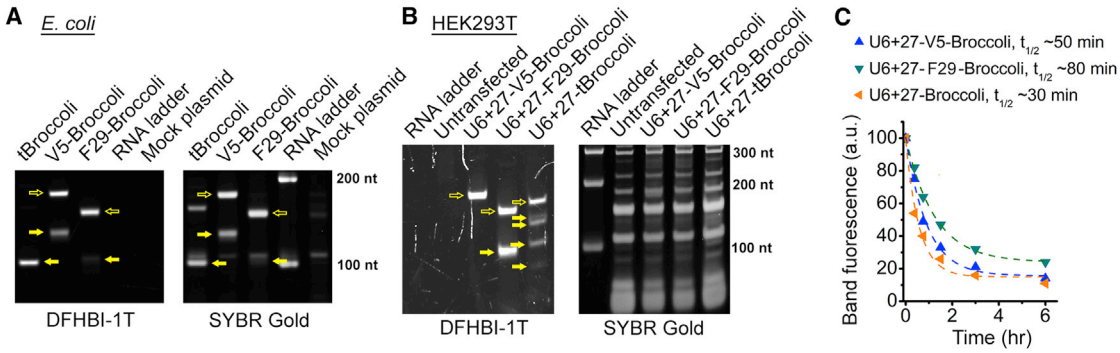

Figure 6. Stability and Cleavage of V5- and F29-Scaffolded Broccoli RNAs in Cells

(A) Test of V5 and F29 scaffold cleavage in bacteria. V5-Broccoli expression in *E. coli* resulted in two bands: one corresponding to the full-length transcript and one that reflects cleavage downstream of the scaffold. F29-Broccoli also showed two bands; however, the shorter, presumably cleaved fragment, was very faint and the full-length product was the major form of the expressed construct. Open arrows indicate full-length products and filled arrows indicate cleaved products.

(B) Expression of V5-Broccoli and F29-Broccoli in HEK293T cells. All constructs were transcribed off the pAVU6+27 plasmid and had the U6+27 leader sequence at the 5′ end and the transcription terminator on the 3′ end. V5-Broccoli showed one band with a size corresponding to the full-length product. No cleavage products were observed. F29-Broccoli showed two bands. The upper band corresponded to the full-length product, while the lower one is potentially the result of a cleavage event. Open arrows indicate full-length products and filled arrows indicate cleaved products.

(C) Half-lives of RNAs containing V5 and F29 scaffolds. HEK293T cells expressing aptamers as described in (B) were treated with actinomycin D. Cells were harvested at the indicated time points and total RNA was analyzed. Broccoli fluorescence was revealed with DFHBI-1T staining (Figure S14) and the band intensity of the full-length transcript was quantified. The intensity of the 5S bands stained with SYBR Gold was used for signal normalization. The numbers were plotted and fitted to a monoexponential decay curve to calculate RNA half-life. An unscaffolded Broccoli was used as a control. The scaffolded RNAs were more stable relative to the unscaffolded RNA. a.u., arbitrary units.

aptamers in cells. To test this, we used flow cytometry to compare the brightness of HEK293T cells expressing unscaffolded Broccoli with cells expressing F29-Broccoli or F30-Broccoli. We found that the mutations did not alter the fluorescence-enhancing properties of the scaffold (Figure S17), while both F29 and F30 provide substantial signal increase compared with unscaffolded Broccoli (Figure 7C; Figure S17). Similar effects were seen in bacteria (Figure S16B). These data suggest that mutations used to create F30 did not impair its scaffolding properties and that the F30 scaffold enhances Broccoli folding in cells.

Our data suggested that V5 is also a bioorthogonal and potentially useful scaffold. To compare F30 with V5 in cells, we expressed V5-Broccoli in HEK293T and analyzed it using flow cytometry (Figure S17). Despite the high expression level, V5-Broccoli shows very modest fluorescent signal in mammalian cells, suggesting that V5-Broccoli fusion folds poorly in cells. The basis for the poor folding is unclear.

One of the exciting properties of F29 is its ability to easily accommodate aptamer insertions into either or both stems (arms) (Figure S13C) (Shu et al., 2014). In the experiments described above, we inserted Broccoli into arm 1. We thus tested if insertion of Broccoli into arm 2 would enable Broccoli fluorescence in cells. Flow cytometry data demonstrate that F30-Broccoli (arm 2) shows fluorescence, although slightly reduced compared with the arm 1 insertion (Figure 7C). Next, we asked if we can use both arms for aptamer insertion. We cloned either two Broccolis (2xBroccoli) or two dimeric Broccolis (dBroccoli, 2xdBroccoli) (Figure S18). Dimeric Broccoli is a single RNA comprising two Broccolis connected in a way so they form one long stem-loop (Filonov et al., 2014). Insertion of Broccoli and especially dBroccoli into both arms of F30 provides a substantial boost in cellular fluorescence (Figure 7C). These results demonstrate the utility of the F30 scaffold for maintaining the structure of aptamers inserted into either or both arms. In addition, F30-2xdBroccoli appears to be a superior tag compared with a single Broccoli tag for RNA tagging in cells.

Finally, we tested if F30-scaffolded probes can be used to create aptamer cassettes, i.e. repetitive identical sequence separated by linkers. The main potential problem with creating cassettes is that individual aptamers can misfold by hybridizing with each other, i.e., inter-aptamer hybridization. This may substantially decrease the number of properly folded aptamers and thus result in few functional aptamers in a cassette. A potential solution to this problem is to use very stable scaffolding elements that would prevent inter-aptamer hybridization, since the efficient folding of the scaffold would dominate over misfolding of aptamers. We engineered an 328-nt long 2x(F30-2xBroccoli) cassette consisting of two F30-2xBroccoli units and tested its cellular fluorescence using. The data showed that the cells were as bright as the ones transfected with a single F30-2xdBroccoli (234 nt). Notably, the size of these cassettes is relatively small, enabling a large number of fluorophores to be added to an RNA without having to append a very large nucleotide sequence. Overall, this suggests that F30 is suitable for expressing tandem RNA aptamers in cassettes.

In-gel staining shows that all F30 Broccoli constructs generated are expressed as single transcripts (Figure S19A). In addition, quantification of the band fluorescence intensities shows that the fluorescence signal increases precisely with the number of additional Broccoli units in a single transcript (Figure S19B). Thus, this shows that there is minimal aptamer misfolding, including in the 2x(F30-2xBroccoli) cassette. These data suggest that F30 can be used as a basis for engineering even longer cassettes that have preserved folding of individual units and thus close to linear signal (or activity) enhancement.

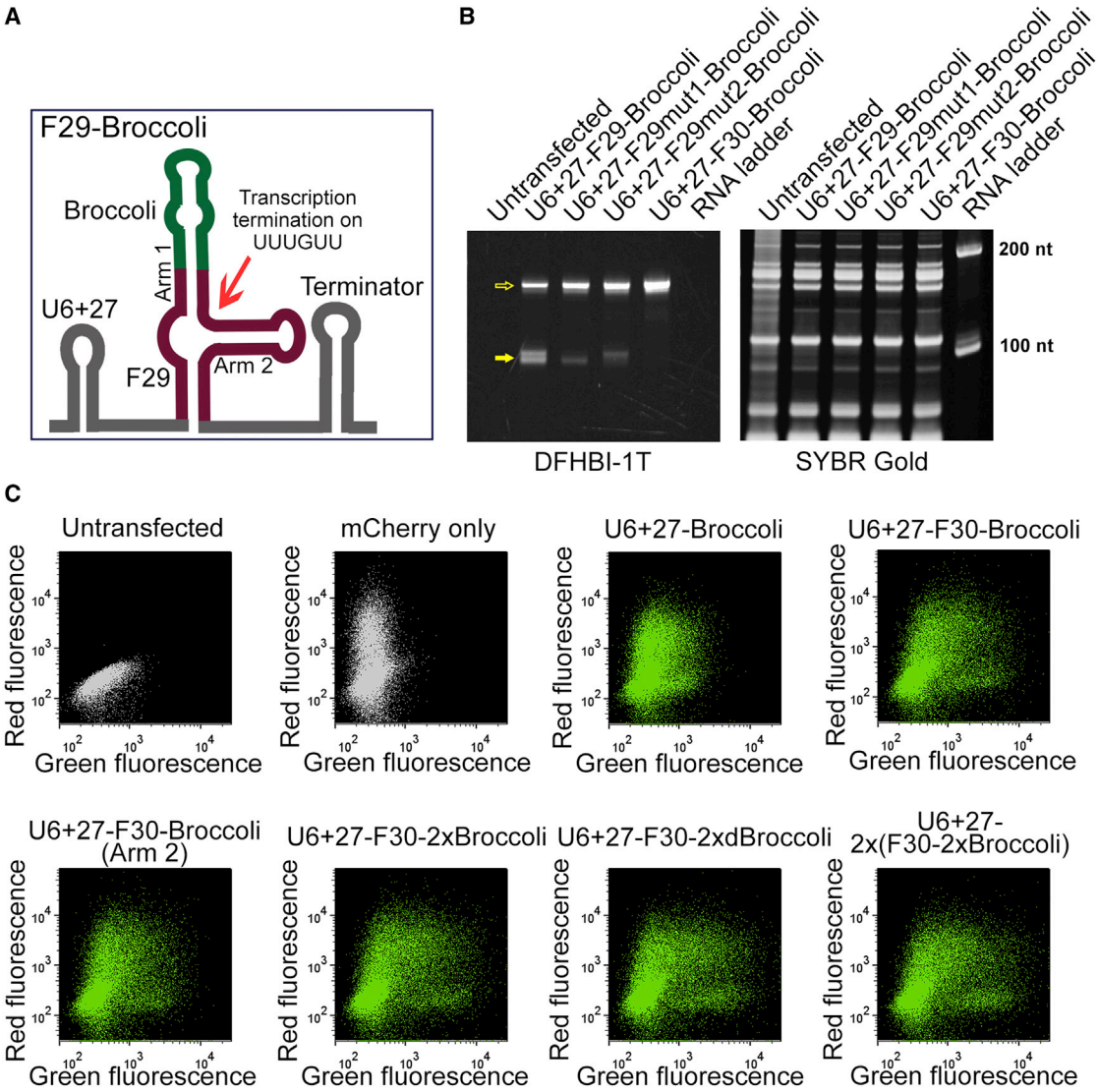

Figure 7. Engineering and Validation of the F30 Scaffold

(A) Schematic representation of U6+27-F29-Broccoli (in arm 1) with the terminator at the 3′ end. We proposed that the lower molecular weight product observed on the gel is a result of an early transcription termination on the UUUGUU sequence (indicated with red arrow).

(B) In-gel staining to identify F29 mutants that do not form the lower molecular weight bands. F29mut1-Broccoli and F29mut2-Broccoli expressed in HEK293T cells showed suppressed formation of either one or the other lower molecular weight band. This allowed us to engineer the final F30 scaffold, which contains mutations found in both F29 variants. F30-Broccoli shows only one major product expressed in cell. Although the total amount of the expressed RNA remained similar in all the lanes, suppressed formation of the unwanted bands lead to higher amount of the desired, full-length transcript. Open arrows indicate full-length products and filled arrows indicate cleaved products.

(C) F30 enhances Broccoli fluorescence in cells and allows engineering of brighter fluorescent tags. Flow cytometry analysis of DFHBI-1T-treated HEK293T cells expressing unscaffolded Broccoli, F30-Broccoli, F30-Broccoli (arm 2), F30-2xBroccoli, F30-2xdBroccoli or 2x(F30-2xBroccoli). mCherry expressed from another plasmid was used for assessing transfection efficiency. Transfected cells were analyzed in the green and red fluorescence channels. F30 substantially improves Broccoli fluorescence signal when compared with unscaffolded Broccoli. Insertion of Broccoli into arm 2 of F30 also generates bright fluorescent signal, which led to engineering of F30 with both arms bearing either two Broccoli or two dimeric Broccolis. All the constructs containing two or more Broccoli units demonstrated significantly increased cellular fluorescent signal.

DISCUSSION

Aptamer scaffolds are important for expressing aptamers and other functional RNAs in cells. However, the effect of the scaffold on RNA stability and scaffold-induced RNA cleavage has not been extensively examined. Here, we systematically examined the cleavage and stability of the commonly used tRNA scaffold and found that it induces cleavage adjacent to the base of the tRNA. This results in decreased RNA stability and overall reduction in RNA levels. This scaffold-induced RNA instability counteracts that purpose of the scaffold, which is to increase the amount of the aptamer that is available in the cell.

$tRNA^{Lys}_3$-scaffolded RNAs may be particularly prone to cleavage, since they fold into the native tRNA structure and likely contain sequence motifs that direct tRNA cleavage (Ponchon and Dardel, 2007). Although the tRNA scaffold is processed in cells, it has been used for scaffolding Spinach and Spinach2 in imaging experiments in mammalian cells (Paige et al., 2011; Strack et al., 2013). However, in each case, the RNA that was tagged with the Spinach/Spinach2-tRNA fusion was an RNA that naturally occurs in clusters or granules in cells. The accumulation of these RNAs into clusters likely enabled the tRNA portion of the Spinach tag to be sequestered from cleavage pathways, enabling the Spinach-tagged RNA to be imaged. However, cleaved products may have added some haziness to the images. In the case of RNAs that are not normally found in clusters, the tRNA would be cleaved, preventing this type of RNA from being imaged using a tRNA-Spinach tag. Thus, scaffolds that are not processed in mammalian cells are essential for imaging nonclustered RNAs using aptamer tags.

Using a novel in-gel imaging system to monitor levels of specific RNAs tagged with Broccoli, we tested two other available scaffolds, V5 and F29. We show that F29 provides the most homogenous aptamer expression in bacteria, while V5 is not associated with RNA cleavage in mammalian cells. F29 is particularly useful, since it efficiently folds into a highly stable structure (Shu et al., 2014). However, for mammalian cells, the F29 scaffold is undesirable, since its expression leads to two major transcripts: a full-length form and a shorter truncated product in cells. The main full-length transcript shows high stability, unlike the tRNA-tagged transcript, which is highly unstable. Since the presence of truncated transcripts can be undesirable, we reengineered F29 to create the F30 scaffold. This new scaffold is expressed in cells as a single major full-length transcript and shows robust cellular fluorescence when fused to Broccoli.

Additional advantages of F30 include that it can present at least two functional aptamers, one in each arm. Thus, F30 is particularly promising for making cassettes containing multiple Broccoli or other aptamers. In principle, a series of identical aptamers separated by short linkers is likely to have poor fluorescence due to inter-aptamer hybridization. Thus, a large cassette containing many aptamers may have only a few that show fluorescence. Using highly stable and efficiently folded scaffolds such as F30 can potentially bypass this problem. Indeed, we generated highly fluorescent F30-2xdBroccoli and 2x(F30-2xBroccoli) tags, which have approximately four times the fluorescence of a single Broccoli. The use of two tandem F30 scaffolds, each presenting two Broccolis, suggests that it may be possible to prepare cassettes with even more tandem F30 scaffolds, resulting in highly bright fluorescence tags.

Although we focused our efforts on reengineering the Φ29 three-way junction for aptamer expression, there are numerous other three-way junctions found in nature (Lescoute and Westhof, 2006). Conceivably, these structures could also be optimized for scaffolding aptamers in living cells. Similarly, the tRNA scaffold could also be mutated to preserve its structure and its ability to function as an aptamer scaffold but to lose its ability to be recognized by cellular nucleases. Thus, other scaffolds could be generated from naturally stable RNA structures.

Our results point to the importance of testing the effect of scaffolds on RNA cleavage and stability. The in-gel staining assay described here provides a simple approach for selectively monitoring the levels and cleavage of a heterologously transcribed RNA that contains a Spinach or Broccoli tag. The sensitivity of the assay is clearly sufficient for detecting RNA expressed using the common Pol III promoters as well as Pol II promoters.

A useful feature of the staining method is the ability to stain with DFHBI and a nonselective nucleic acid-staining dye. In some cases, the heterologous RNA can be seen with SYBR Gold staining due to its high expression level. Definitive identification of the band is achieved by selective detection in the transfected cells and not the control cells after SYBR Gold staining. An additional advantage of staining with SYBR Gold is that the scaffold-induced folding efficiency of the Broccoli aptamer in the gel can be assessed. Normalization of the fluorescence seen in the DFHBI stained gel to the fluorescence seen in the SYBR Gold stained gel can provide an assessment of folding efficiency. It remains to be seen if the efficiency of Broccoli folding in the context of different scaffolds will be predictive of the folding of other types of aptamers inserted into these scaffolds.

It should be noted that cleavage products that do not contain the Broccoli tag are not detectable in this assay. In addition, it is possible that some RNAs that appear to be cleavage products could be generated through cryptic scaffold-induced transcription initiation or termination sites.

The in-gel staining approach could potentially be useful for other purposes. We were able to follow individual tRNA processing steps and assign their temporal order of cleavage. Similarly, RNA processing reactions can be measured using Broccoli-tagged RNAs in nuclear extracts.

Usually, these experiments are performed using northern blotting, or in the case of nuclear extracts, radiolabeled RNAs. While the sensitivity of northern blotting is still much higher than that of the DFHBI staining (100 fg versus 100 pg), the latter approach has its own distinct advantages. Northern blotting is substantially more laborious and time consuming. On the other hand, DFHBI staining takes 30 min from the time PAGE is completed to obtaining a fluorescent image. This approach is also very inexpensive (see Experimental Procedures for calculations).

The simplicity of the DFHBI staining approach makes the use of Broccoli- or Spinach-tagged RNAs an attractive alternative for RNA labeling over radiolabeling. Subsequent destaining and staining with SYBR Gold or another nonselective RNA dye is useful to confirm the quality and amount of the cellular RNA.

SIGNIFICANCE

RNA aptamers have the potential to be an important tool for regulating cell function and for imaging cellular processes. However, aptamers often fold poorly in cells and therefore require RNA scaffolds that promote their efficient folding. Scaffolded aptamers can then be expressed in cells either on their own or appended to other RNAs in the form of fusion RNAs. However, the effects of the scaffold on RNA stability are unknown. We developed a simple in-gel staining approach to rapidly characterize the expression level and RNA cleavage of Spinach- or Broccoli-tagged RNAs. This approach allows tagged RNAs to be rapidly detected, with

 ©2015 Elsevier Ltd All rights reserved

high sensitivity and specificity in cellular RNA preparations. Using this approach, we found that the tRNA aptamer scaffold is rapidly targeted by endonucleases, leading to RNA cleavage, degradation, and instability. We show that other scaffolds can be used to express aptamer RNA fusions and bypass these undesirable effects. In addition, we reengineered a previously reported three-way junction scaffold to create a new one, F30, which we found to promote the folding of RNA aptamers in cells. These results show that RNA processing events can be rapidly characterized using Spinach- or Broccoli-tagged RNA and identify scaffolds that enable efficient heterologous aptamer expression and tagging in cells.

EXPERIMENTAL PROCEDURES

In-Gel Imaging of Fluorescent RNAs

Total bacterial or mammalian cell RNA was purified using Trizol LS reagent (Life Technologies) following the manufacturer's protocol. Typically 200–500 ng of total bacterial RNA, 2–5 μg of mammalian cell RNA or 50–100 ng of in vitro transcribed RNA was loaded into a well of precast 6% Tris/borate/EDTA (TBE) Gel or 6% or 10% TBE-Urea Gel (Life Technologies) and ran at 270–300 V in 1× TBE buffer. RiboRuler Low Range RNA Ladder (Thermo Scientific) or Low Range ssRNA Ladder (NEB) was used as a molecular weight standard.

After electrophoresis, the gel was washed 3 × 5 min with water and then stained for 10–30 min in 10 μM DFHBI or DFHBI-1T in buffer containing 40 mM HEPES (pH 7.4), 100 mM KCl, 1 mM $MgCl_2$. Then the gel was imaged using a ChemiDoc MP (Bio-Rad) with 470 ± 15 nm excitation and 532 ± 14 nm emission. Next, to see all the RNA in the sample, the gel was again washed 3 × 5 min with water followed by staining for 30 min with SYBR Gold fluorophore (Life Technologies) diluted 1/10,000 in TBE buffer. Then, gel was imaged under the same instrument using the preset SYBR Gold channel (302 nm excitation and 590 ± 55 nm emission). Gel band intensities were quantified using Image Lab 5.0 software (Bio-Rad). The bacterial or mammalian 5S rRNA band was used for loading normalization.

Cost Comparison for Northern Blotting and DFHBI-1T In-Gel Staining

The cost was calculated for a NorthernMax Kit (Life Technologies) for the blotting, which uses 5 × 5 cm membrane, with 1,000 cm^2 of membrane sold for $469. Only kit and membrane cost $11.7 per blot. DFHBI-1T can be purchased from Lucerna Technologies (New York) for $399.99 per 5 mg. 15 ml of 10 μM DFHBI-1T solution can be used for up to five stainings. This makes the cost ~$0.80 per gel.

Other methods can be found with this article in the Supplemental Information.

SUPPLEMENTAL INFORMATION

Supplemental Information includes Supplemental Experimental Procedures and 19 figures and can be found with this article online at http://dx.doi.org/10.1016/j.chembiol.2015.04.018.

AUTHOR CONTRIBUTIONS

G.S.F. and S.R.J. conceived and designed the experiments. W.S. synthesized the fluorophores. G.S.F. performed the experiments and analyzed the data, with the assistance of C.W.K. G.S.F. and S.R.J. wrote the manuscript.

ACKNOWLEDGMENTS

We thank M. You, R.S. Strack, and H. Kim for useful comments and suggestions. We are grateful to J. McCormick and S.Z. Merlin (Department of Pathology and Laboratory Medicine cell sorter core) for their help with flow cytometry. We also thank L.-L. Chen (Shanghai Institutes for Biological Sciences, China) for the pZW1-sno vector. This work was supported by NIH grants to S.R.J. (R01 NS064516 and R01 EB010249). In addition, the authors disclose that S.R.J. and G.S.F. are authors of a patent application (provisional patent USPTO# 61/874,819) related to technology described in this article.

Received: November 26, 2014
Revised: April 14, 2015
Accepted: April 20, 2015
Published: May 21, 2015

REFERENCES

Chang, Z., Westaway, S., Li, S., Zaia, J.A., Rossi, J.J., and Scherer, L.J. (2002). Enhanced expression and HIV-1 inhibition of chimeric tRNA(Lys3)-ribozymes under dual U6 snRNA and tRNA promoters. Mol. Ther. *6*, 481–489.

Culler, S.J., Hoff, K.G., and Smolke, C.D. (2010). Reprogramming cellular behavior with RNA controllers responsive to endogenous proteins. Science *330*, 1251–1255.

Filonov, G.S., Moon, J.D., Svensen, N., and Jaffrey, S.R. (2014). Broccoli: rapid selection of an RNA mimic of green fluorescent protein by fluorescence-based selection and directed evolution. J. Am. Chem. Soc. *136*, 16299–16308.

Good, P.D., Krikos, A.J., Li, S.X., Bertrand, E., Lee, N.S., Giver, L., Ellington, A., Zaia, J.A., Rossi, J.J., and Engelke, D.R. (1997). Expression of small, therapeutic RNAs in human cell nuclei. Gene Ther. *4*, 45–54.

Han, K.Y., Leslie, B.J., Fei, J., Zhang, J., and Ha, T. (2013). Understanding the photophysics of the spinach-DFHBI RNA aptamer-fluorogen complex to improve live-cell RNA imaging. J. Am. Chem. Soc. *135*, 19033–19038.

Huang, H., Suslov, N.B., Li, N.S., Shelke, S.A., Evans, M.E., Koldobskaya, Y., Rice, P.A., and Piccirilli, J.A. (2014). A G-quadruplex-containing RNA activates fluorescence in a GFP-like fluorophore. Nat. Chem. Biol. *10*, 686–691.

Kotula, J.W., Sun, J., Li, M., Pratico, E.D., Fereshteh, M.P., Ahrens, D.P., Sullenger, B.A., and Kovacs, J.J. (2014). Targeted disruption of beta-arrestin 2-mediated signaling pathways by aptamer chimeras leads to inhibition of leukemic cell growth. PLoS One *9*, e93441.

Lescoute, A., and Westhof, E. (2006). Topology of three-way junctions in folded RNAs. RNA *12*, 83–93.

Lubitz, I., Zikich, D., and Kotlyar, A. (2010). Specific high-affinity binding of thiazole orange to triplex and G-quadruplex DNA. Biochemistry *49*, 3567–3574.

Martell, R.E., Nevins, J.R., and Sullenger, B.A. (2002). Optimizing aptamer activity for gene therapy applications using expression cassette SELEX. Mol. Ther. *6*, 30–34.

Morl, M., and Marchfelder, A. (2001). The final cut. The importance of tRNA 3′-processing. EMBO Rep. *2*, 17–20.

Muller, M., Heym, R.G., Mayer, A., Kramer, K., Schmid, M., Cramer, P., Urlaub, H., Jansen, R.P., and Niessing, D. (2011). A cytoplasmic complex mediates specific mRNA recognition and localization in yeast. PLoS Biol. *9*, e1000611.

Paige, J.S., Wu, K.Y., and Jaffrey, S.R. (2011). RNA mimics of green fluorescent protein. Science *333*, 642–646.

Paul, C.P., Good, P.D., Li, S.X., Kleihauer, A., Rossi, J.J., and Engelke, D.R. (2003). Localized expression of small RNA inhibitors in human cells. Mol. Ther. *7*, 237–247.

Phizicky, E.M., and Hopper, A.K. (2010). tRNA biology charges to the front. Genes Dev. *24*, 1832–1860.

Ponchon, L., and Dardel, F. (2007). Recombinant RNA technology: the tRNA scaffold. Nat. Methods *4*, 571–576.

Ponchon, L., Catala, M., Seijo, B., El Khouri, M., Dardel, F., Nonin-Lecomte, S., and Tisne, C. (2013). Co-expression of RNA-protein complexes in *Escherichia coli* and applications to RNA biology. Nucleic Acids Res. *41*, e150.

Pothoulakis, G., Ceroni, F., Reeve, B., and Ellis, T. (2014). The spinach RNA aptamer as a characterization tool for synthetic biology. ACS Synth. Biol. *3*, 182–187.

 ©2015 Elsevier Ltd All rights reserved

Renaud de la Faverie, A., Guedin, A., Bedrat, A., Yatsunyk, L.A., and Mergny, J.L. (2014). Thioflavin T as a fluorescence light-up probe for G4 formation. Nucleic Acids Res. *42*, e65.

Schramm, L., and Hernandez, N. (2002). Recruitment of RNA polymerase III to its target promoters. Genes Dev. *16*, 2593–2620.

Seiwert, S.D., Stines Nahreini, T., Aigner, S., Ahn, N.G., and Uhlenbeck, O.C. (2000). RNA aptamers as pathway-specific MAP kinase inhibitors. Chem. Biol. *7*, 833–843.

Shu, D., Khisamutdinov, E.F., Zhang, L., and Guo, P. (2014). Programmable folding of fusion RNA in vivo and in vitro driven by pRNA 3WJ motif of phi29 DNA packaging motor. Nucleic Acids Res. *42*, e10.

Song, W., Strack, R.L., Svensen, N., and Jaffrey, S.R. (2014). Plug-and-play fluorophores extend the spectral properties of Spinach. J. Am. Chem. Soc. *136*, 1198–1201.

Stoltenburg, R., Reinemann, C., and Strehlitz, B. (2007). SELEX–a (r)evolutionary method to generate high-affinity nucleic acid ligands. Biomol. Eng. *24*, 381–403.

Strack, R.L., Disney, M.D., and Jaffrey, S.R. (2013). A superfolding Spinach2 reveals the dynamic nature of trinucleotide repeat RNA. Nat. Methods *10*, 1219–1224.

Tuma, R.S., Beaudet, M.P., Jin, X., Jones, L.J., Cheung, C.Y., Yue, S., and Singer, V.L. (1999). Characterization of SYBR Gold nucleic acid gel stain: a dye optimized for use with 300-nm ultraviolet transilluminators. Anal. Biochem. *268*, 278–288.

Warner, K.D., Chen, M.C., Song, W., Strack, R.L., Thorn, A., Jaffrey, S.R., and Ferre-D'Amare, A.R. (2014). Structural basis for activity of highly efficient RNA mimics of green fluorescent protein. Nat. Struct. Mol. Biol. *21*, 658–663.

Weigand, J.E., and Suess, B. (2007). Tetracycline aptamer-controlled regulation of pre-mRNA splicing in yeast. Nucleic Acids Res. *35*, 4179–4185.

Wilusz, J.E., Freier, S.M., and Spector, D.L. (2008). 3′ end processing of a long nuclear-retained noncoding RNA yields a tRNA-like cytoplasmic RNA. Cell *135*, 919–932.

Yin, Q.F., Yang, L., Zhang, Y., Xiang, J.F., Wu, Y.W., Carmichael, G.G., and Chen, L.L. (2012). Long noncoding RNAs with snoRNA ends. Mol. Cell *48*, 219–230.

Zhang, X., Potty, A.S., Jackson, G.W., Stepanov, V., Tang, A., Liu, Y., Kourentzi, K., Strych, U., Fox, G.E., and Willson, R.C. (2009). Engineered 5S ribosomal RNAs displaying aptamers recognizing vascular endothelial growth factor and malachite green. J. Mol. Recognit. *22*, 154–161.

Zhang, H., Endrizzi, J.A., Shu, Y., Haque, F., Sauter, C., Shlyakhtenko, L.S., Lyubchenko, Y., Guo, P., and Chi, Y.I. (2013). Crystal structure of 3WJ core revealing divalent ion-promoted thermostability and assembly of the Phi29 hexameric motor pRNA. RNA *19*, 1226–1237.

 ©2015 Elsevier Ltd All rights reserved